International Journal of Nanomedicine Dovepress

Open Access Full Text Article ORIGINAL RESEARCH

Desferrioxamine-Laden Nanofibrous Scaffolds with Efficient Angiogenesis for Accelerating Diabetic Wound Healing

Yang Zhao[1,2,*], Jialong Chen[1,2,*], Muran Zhou[1,2], Guo Zhang[1,2], Wenhao Wu[1,2], Zhenxing Wang[1,2], Jiaming Sun[1,2], Aimei Zhong[1,2]

[1]Department of Plastic Surgery, Union Hospital, Tongji Medical College, Huazhong University of Science and Technology, Wuhan, 430022, People's Republic of China; [2]Wuhan Clinical Research Center for Superficial Organ Reconstruction, Wuhan, 430022, People's Republic of China

*These authors contributed equally to this work

Correspondence: Aimei Zhong; Jiaming Sun, Department of Plastic Surgery, Union Hospital, Tongji Medical College, Huazhong University of Science and Technology, 1277 Jiefang Avenue, Wuhan, 430022, People's Republic of China, Tel +86-13317174169; +86-13986246496, Fax +86-027-85726240, Email aimei_zhong@hust.edu.cn; sunjm1592@sina.com

Background: Delayed diabetic wound healing is one of the clinical difficulties, the main reason is the limited angiogenesis ability. Deferriamine (DFO) is an iron chelating agent that can induce angiogenesis, but its application is limited due to its short half-life. Increasing the load and slow release performance of desferriamine is beneficial to accelerate diabetic wound healing.

Materials and Methods: In this study, we developed collagen (Col)-graphene oxide (GO) and (1% w/w) DFO-loaded nanofiber electrospinning scaffolds (DCG) using the electrospinning technique. We tested the physicochemical properties, drug release performance, and vascularization biological function of the scaffolds, and finally evaluated the promotion of full-thickness wound healing in the diabetic rat models.

Results: The results showed that DCG scaffolds have good mechanical properties and water-holding capacity and can release DFO continuously for 14 days. In vitro, the novel DCG scaffold exhibited good biocompatibility, with the up-regulation at the gene level of VEGF and its regulator HIF-1α, promoters of angiogenesis. This was verified in vivo, as the scaffold enhanced granulation tissue formation and improved neovascularization, thereby accelerating wound healing when applied to full-thickness defects on the back of diabetic rats.

Conclusion: The DCG nanofiber scaffold prepared in this study has good biocompatibility and vascularization ability, and improves the microenvironment in vivo, and has a good application prospect in diabetic wound repair.

Keywords: diabetic wounds, angiogenesis, desferrioxamine, graphene oxide, electrospinning, drug release

Introduction

The epidemic of diabetes mellitus and its complications poses a major global health threat.[1] Among 3 million diabetes-related hospitalizations in the United States, 20% of the cases are complicated with diabetic wounds and especially diabetic foot ulcers,[2] while about 20% of moderate and severe diabetic foot ulcer infections lead to amputation.[3] In all, this yields great challenges not only to the patients, but to the global healthcare system. Contrary to the four overlapping stages of hemostasis, inflammation, proliferation, and re-epithelialization observed during acute wound healing, the diabetic wound reveals altered and complex figures that delay the healing process.[4] Particularly, diabetic wounds are characterized by inadequate vascularization caused by hyperglycemia, which restricts the supply of nutrients and oxygen to the wound site, thereby compromising new tissue formation and delaying wound healing.[5,6] Hence, one of the most important strategies in diabetic wound management is to promote revascularization in the affected region.

In optimal physiological conditions, angiogenesis is influenced by a variety of growth factors.[7] Listed as one of the most crucial among those, the vascular endothelial growth factor (VEGF) is primarily regulated by hypoxia-inducible

Received: 24 July 2024
Accepted: 6 October 2024
Published: 17 October 2024

factor (HIF)-1α.[8] In the acute hypoxic environment ensuing tissue wounding and damage, the release of HIF-1α is brought about by hypoxia and derives from the various cellular actors of wound healing including endothelial cells, fibroblasts, and macrophages during the initial stage of wound healing;[9] HIF-1α then enters the nucleus of target cells and dimerizes into HIF-1β, which enables its binding to the hypoxic reaction element. This results in the upregulation and activation of more than 60 hIF-1α target genes for tissue repair, cell growth and proliferation, and upregulation of VEGF.[10] However, in diabetic wounds, topical deposition of free iron results in excessive degradation of HIF-1α by prolyl 4-hydroxylase (PHD) enzymes that require iron (Fe^{2+}) as a cofactor,[11] further impeding the wound healing conditions. Hence, in current medicine, a therapeutic measure that would maintain the activity of HIF-1α in the context of diabetic wounds is highly desirable.

Desferrioxamine (DFO) is a small molecule chelating chemical that is approved by the FDA as an iron chelator to treat thalassemia or iron poisoning. Topical application of DFO as an iron chelating agent and a stabilizer of HIF-1α accumulation is an effective method to promote tissue angiogenesis, through the upregulation of the expression of many growth factors such as VEGF and stromal cell-derived factor-1α (SDF-1 α). Because of this function, DFO has been used to improve bone and skin tissue regeneration.[12–14] However, application to diabetic wound healing has been limited by the cell and tissue toxicity of DFO and its short half-life that prevents sustained treatment effects,[15,16] requiring the development of biocompatible delivery vehicles with the ability to sustain-release the DFO and enable prolonged treatment as required in the case of diabetic wounds.

Collagen (Col), of which type I is the most abundant, is the main component of skin extracellular matrix (ECM); It possesses good biocompatibility, hydrophilicity, and low immunogenicity.[17,18] It can regulate cell phenotypes and cell-ECM interactions, and alter the physico-chemical properties of scaffolds to improve the rate and quality of wound healing.[19] Collagen is easy to extract and process and has been prepared into a variety of structures for wound dressing such as hydrogels, sponges, and nanofibers.[20] However, collagen has poor mechanical properties and pure collagen-based materials are easy to break,[21] which makes it difficult to prepare self-standing materials. Because of its high hardness, graphene Oxide (GO) is often used to improve the mechanical properties of scaffolds;[22–24] In fact, the tensile strength and Young's modulus of the composite scaffold can be improved when as reinforcement, GO is evenly and thoroughly distributed within the main matrix compounds.[25]

Researchers have tried to solve the problem of long-term stable drug delivery through a variety of nanotechnology, but the first key is to choose a reasonable drug carrier, which should have good compatibility with the loaded drug.[26] Then there is the practicality of nanotechnology, in general, there are two approaches to nanotechnology, one is the bottom-up approach, such as self-assembly and chemical synthesis.[27] The other is the top-down approach, such as electrospinning.[28] Electrospinning technology has great potential for loading bioactive substances, mainly because of the high porosity, large specific surface area, and suitable mechanical strength of nanofiber membranes, so that bioactive substances can be uniformly dispersed on the surface or inside the nanofiber.[29,30] In addition, electrospinning has evolved from single fluid[31] to coaxial,[32] side-by-side,[33] triaxial,[34] Janus,[35] and combined. This provides a simple and practical method to control the morphology and structure of nanofibers using different raw materials or modified materials.[36] The nanonetwork structure of nanofiber membranes is very similar to the skin's natural extracellular matrix (ECM) and can serve as a carrier for the controlled delivery and release of biomolecules and drugs, expanding their application in the field of wound healing.[37] In this study, we developed a drug-loaded electrospinning scaffold. Using collagen and graphene oxide as matrix materials, the nanofiber scaffold containing DFO was prepared by electrospinning. Then, the physicochemical properties, sustained drug release performance, biocompatibility, and angiogenesis of the stent were evaluated in vitro. Finally, the wound healing and vascularization effects of the DCG composite scaffold were further evaluated in the full-thickness diabetic rat wound model. The diagram showing the experimental design is shown in Figure 1.

Materials and Methods

Materials

All utilized chemicals were of analytical grade and pure. Type I collagen was procured from Kele Biotech (Chengdu, China), graphene oxide was obtained from Suzhou Tanfeng Tech (China), and desferrioxamine (DFO) was purchased

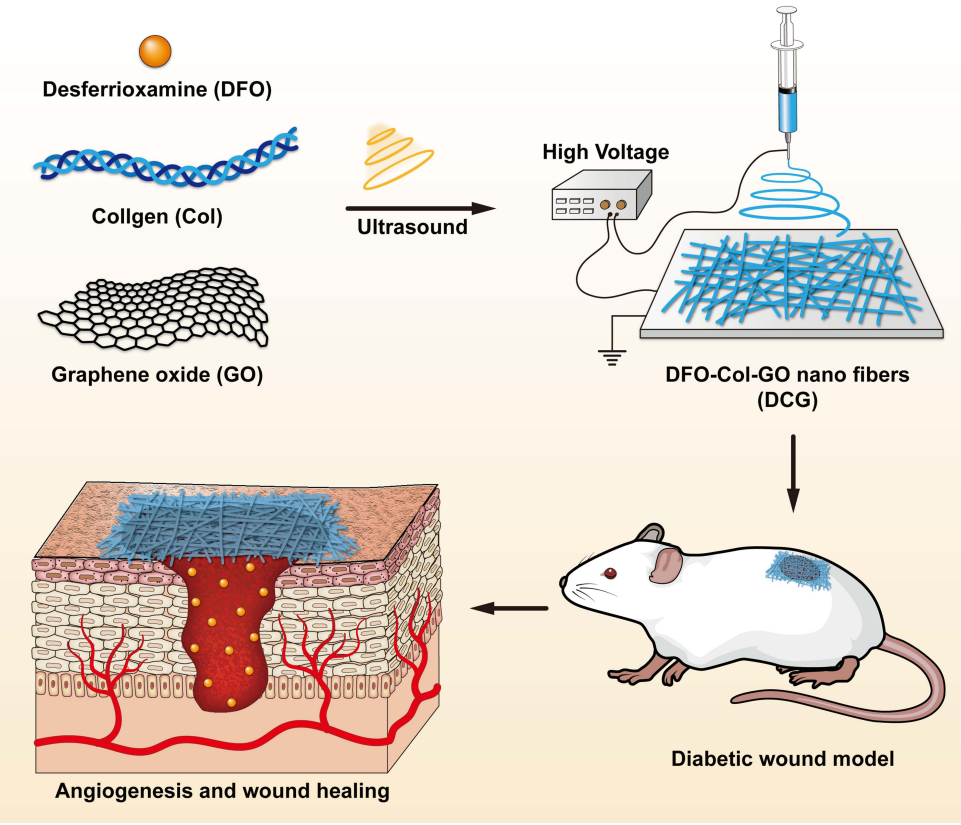

Figure 1 Schematic illustration of the fabrication procedure of DCG and its application on diabetic wound model.

from Shanghai Yuanye Biotechnology Co., Ltd. (located in Shanghai, China). Dulbecco's modified Eagle's medium (DMEM) and Roswell Park Memorial Institute 1640 (RPMI 1640) were procured from Hyclone (USA). Fetal bovine serum (FBS), penicillin-streptomycin (PS), and other cell culture reagents were obtained from Gibco (USA). Furthermore, Calcein Acetoxymethyl Ester/propidium iodide (Calcein AM/PI) and Cell Counting Kit-8 (CCK-8), along with hematoxylin-eosin and Masson's trichrome kits, were obtained from Sigma-Aldrich. Matrigel was purchased from BD (USA).

Fabrication of the DFO-Col-GO Nanofiber Scaffolds

To prepare the DFO-Col-GO (DCG) scaffolds, 240 mg of Col, 0.48 mg of GO, and 2.4 mg of DFO were dissolved in 4 mL of hexafluoroisopropanol (HFIP). The resulting solution, which contained desferrioxamine-col-GO/HFIP, was subjected to electrospinning at 25–27 kV using a 17G needle. The extrusion speed was maintained at 0.5 mL/h, and the spinneret was separated from the collector (aluminum mesh) by 15 cm. The samples were cooled to −20°C and freeze-dried in a vacuum lyophilizer, resulting in the formation of DCG nanofiber scaffolds. Finally, the samples were cut into 1 cm diameter disks, placed in 12-well plates, and sterilized overnight by exposure to ultraviolet light.

Using the same procedures, collagen-only scaffolds (Col) and collagen-GO hybrid scaffolds (CG) were also obtained.

Morphological Characterization

The freeze-dried nanofiber scaffolds were coated with gold nanoparticles and examined using scanning electron microscopy (SEM, JSM-IT300, JEOL, Japan) at a high voltage of 20 kV to observe their microstructure, after obtaining high-resolution SEM images of the electrospun scaffolds, the diameters of the nanofibers were measured using image analysis software (Image J).

Freeze-dried products were also used for ^{1}H NMR spectroscopy (Varian, 600 MHz), attenuated total reflection-Fourier transform infrared spectroscopy (ATR-FTIR), and Raman spectroscopy (VERTEX 70, Bruker, Germany) using LabRAM HR800 (HORIBA JobinYvon, France) for recording the surface characteristics of the scaffolds. FTIR measurements were carried out at a resolution of 4 cm^{-1} in the frequency range of 4000–500 cm^{-1} and the Raman spectrum was recorded at a scanning range of 50–4000 cm^{-1}. The excitation source was a diode laser with a wavelength of 532 nm adjusted to a power of 30 mW. All data were then analyzed in OriginPro 2019 (OriginLab, America).

Mechanical Testing of the Scaffolds

An all-electric dynamic test instrument (ASTM D638, Instron) was used to measure the mechanical properties of the scaffolds. Tensile tests were conducted on the scaffolds with a cell load of 20N and extension speeds of 5 mm/min. The mechanical properties including Young's moduli and stress-strain curves, were calculated using the OriginPro software.

Water Contact Angle Measurements, Water Absorption, and Retention Capacity

The water contact angle was measured using a contact angle analyzer (JGW-360B, China) to evaluate the hydrophilicity of the fabricated nanofibrous scaffolds. A volume of 0.2 μL of pure water was dispensed onto the surface of each sample, followed by an analysis of the contact angle using the instrument's software. Each experimental group was tested with three replicates.

To determine the water absorbability, five specimens of each scaffold type were initially weighed (W_0) and immersed in phosphate-buffered saline (PBS) at 37 °C for 24 hours. Subsequently, the specimens were taken out from the PBS and reweighed to determine Wt. The percentage of weight absorbed was calculated using the following formula:

$$\text{Water absorption } (\%) = (W_t - W_0)\, W_0 \times 100\%$$

A filter with 0.5 mm holes was employed to hold the wet samples. After centrifugation (AccuSpin 400, Fisher Scientific) at 260 g for 5 minutes at room temperature, the weight of the samples was measured as W_1 and water retention was determined using the following formula:

$$\text{Water retention } (\%) = (W_1 - W_0)\, W_0 \times 100\%$$

In vitro DFO Release

Each scaffold sample was immersed in a 20 mL solution of PBS with a pH of 7.4 at a temperature of 37 °C and agitated until maximum drug release was achieved. After being mixed with a specified quantity of FeCl3, the amount of DFO that was released was measured by recording the absorbance at a wavelength of 485 nm using a UV-Vis spectrophotometer at regular intervals, as per the standard DFO sodium calibration curve. Release experiments were conducted in triplicate, and the average value was recorded.

In vitro Cell Experiments

Human dermal fibroblasts (HDF) and GFP-HUVECs (ATCC, USA) were cultured in growth media enriched with DMEM and RPMI 1640 respectively, supplemented with 10% fetal bovine serum and 1% penicillin/streptomycin at 37°C and 5% CO_2 in a humidified incubator. Cell detachment was achieved using 0.05% trypsin, and media was replenished every 2 days.

The scaffolds were sterilized using UV and immersed in RPMI 1640 for 24 hours. The media was then collected and centrifuged at 1000 rpm for 5 minutes and filtered through a 0.20 μM syringe filter. The resulting filtered media, which served as the extract liquor of the scaffold, was collected for cytology experiments.

Cytocompatibility Testing

The scaffolds were sectioned into circular shapes with a diameter of 1 cm and placed in 24-well plates, following which they were sterilized using UV light for an entire night. Next, HDF cells were seeded in different samples at a concentration of $1*10^4$ cells per sample and cultured for 5 days to assess the cytocompatibility of the scaffolds.

Live/dead assays were then conducted, and cells were stained with Calcein AM/PI, following the manufacturer's protocol. The visualization of cells was performed using a confocal laser microscope (Leica Microsystems, Germany). The proliferation of cells on the scaffold was assessed after 1, 3, and 5 days of incubation using the CCK-8 assay. To perform the assay, 100 μL of CCK-8 working solution was added to each well after replenishing the medium, and the culture was then incubated at 37°C for 1 hour. Afterward, 100 μL of the supernatant was transferred to new 96-well plates, and their optical density (OD) values were measured at 450 nm using a microplate reader (BioTek ELx800, USA).

Tube Formation Assay

For the tube formation assay, 50 μL of thawed Matrigel was added to each pre-cooled well of a 96-well plate and incubated for 1 hour at 37°C. Next, GFP-HUVECs were seeded with a density of 1×10^4 cells per well into the Matrigel-coated wells, and the extract liquor obtained from the different scaffolds was used to treat the cells. After 6 hours of incubation, each well was imaged using a confocal laser scanning microscope, and the images were quantified using ImageJ software.

Cell Migration Assay

For the cell migration assay, GFP-HUVECs were seeded in 24-well plates at a density of 5×10^4 cells per well and cultured until they reached a 90% confluence. Scratch wounds were then carefully created on the cell monolayers using a 200 μL pipette tip, followed by a gentle rinse with phosphate-buffered saline (PBS). Subsequently, the medium in each well was substituted with a different extract liquor. At 0, 8, 16, and 24 hours of incubation, images of the scratched wounds were captured and the area of the remaining wound was measured at each time point using the Image J software.

RT-PCR Analysis

The mRNA expression levels of hypoxia-inducible factor 1-alpha (HIF-1α) and vascular endothelial growth factor (VEGF) in the GFP-HUVECs treated with different extract liquors were determined through real-time polymerase chain reaction (RT-PCR). Total RNA extraction from the cultured GFP-HUVECs was achieved using the Trizol reagent, and reverse transcription was carried out using the Revert Aid First Strand cDNA Synthesis Kit. The primer sequences used are shown in Table 1.

The AceQ Universal SYBR qPCR Master Mix was utilized in the RT-PCR, and a real-time PCR system was employed to quantify the PCR products. The amplification conditions were as follows: 95°C for 5 min, 95°C for 10s, and 60°C for 30s (40 cycles). The mRNA expression level in all experimental groups was calculated using the $2^{-\Delta\Delta CT}$ method.

In vivo Wound-Healing Studies

The experimental procedures of this study were granted ethical approval by the Animal Ethical Committee of Huazhong University of Science and Technology (HUST). All animals followed the principles of the "Guide for the Care and Use of Laboratory Animals" and "The Guidance to Experimental Animal Welfare and Ethical Treatment" established by the National Science Council of China.

Table 1 Primers for qRT-PCR in This Study

Target Gene	Direction	Sequence
HIF-1α	F	TGATTGCATCTCCATCTCCTACC
	R	GACTCAAAGCGACAGATAACACG
VEGF	F	CCCACTGAGGAGTCCAACATC
	R	TACACGCTCCAGGACTTATACCG

STZ-Induced Diabetic Models

Six male Sprague-Dawley (SD) rats, aged six weeks and weighing an average of 180–200 g, were acclimatized in a temperature and humidity-controlled room for one week. After an overnight fast, streptozotocin was administered to the rats in the right upper abdomen. Rats with a fasting glucose level of > 11.1 mmol/L for three consecutive days were deemed to have developed diabetes mellitus (DM). Otherwise, STZ was injected again until the DM model was successfully established.

In vivo Wound-Healing Assay

To anesthetize the six diabetic rats, 3% pentobarbital sodium (0.1mL per 100g) was administered via intraperitoneal injection and their dorsal fur was shaved. The incision area was marked with methylene blue and subsequently disinfected with iodophor. Three full-thickness wounds, each with a diameter of 10 mm, were randomly created on each side of the dorsal central line in the experimental animals. Wounds in each rat were treated with Col, CG, and DCG in a random order. Subsequently, the wound area was fixed with a medical bandage that was changed every two days. Wound images were captured using a Canon digital camera on days 0, 3, 7, 10, and 14 post-surgery. Image J software was utilized to quantify the surface area of the wound at each time point. The rate of wound closure was then calculated using the following formula:

$$\text{Wound closure rate } = (S_0 - S_n)/S_0 * 100\%$$

Where S_0 refers to the original wound area and S_n denotes the area of the wound at days 0, 3, 7, 10, and 14 post-surgeries.

Histological Analysis

On day 14 post-surgery, all experimental rats were sacrificed using an overdose of anesthetics, and tissues from both unwounded and wounded areas were harvested and fixed in 10% formaldehyde. Hematoxylin-Eosin (H&E) and Masson's trichrome staining were performed on wound tissue samples obtained on day 14 post-surgery to evaluate epidermal, collagen, and new tissue generation. Furthermore, an immunohistochemical staining using antibodies against specific CD31 was employed to observe vascular endothelial cells. An optical microscope (Nikon H600L, Tokyo, Japan) was utilized for cell examination and image capture.

Statistical Analyses

The normal distribution of the data was assessed, and all results that met the normal were expressed as mean ± standard deviation. Student's *t*-test and ANOVA were performed on the data using GraphPad Prism 9.5, and the difference was statistically significant ($p < 0.05$) or not ($p > 0.05$). Non-normal data were presented as medians and interquartile intervals using non-parametric tests.

Results

DCG is prepared from a mixed solution of DFO, Col, and GO. CG is prepared from a mixed solution of Col and GO. Col is prepared from a pure Col solution. From a macroscopic view (Figure 2A-C), no significant difference was detected among groups. Advanced analysis by scanning electron microscopy (SEM) (Figure 2D–I) then revealed randomly organized networks of nanofibers presenting a smooth surface of the fibers, forming 3D structures with high porosities and interconnected pores. For all groups, most fibers presented a diameter between 100 and 500 nm (Figure 2J-L), which is propitious for cell attachment and growth.[38]

We used FTIR spectroscopy to confirm the chemical structures of the scaffolds and these results are shown in Figure 2M. In the FTIR spectra, the -NH stretching vibration was detected as the peak at 3367 cm^{-1}, these were derived from the $-NH_2$ and C-N groups in all samples. Further, peaks at 1637, 1542, and 1450 cm^{-1} were assigned to the C=O stretching, N-H bonding, and C-N stretching of amide ($-CONH_2$) linkages in collagen, respectively. As the functional groups of DFO are like those found in collagen, characteristic absorption peaks for DFO could not be specified.[39]

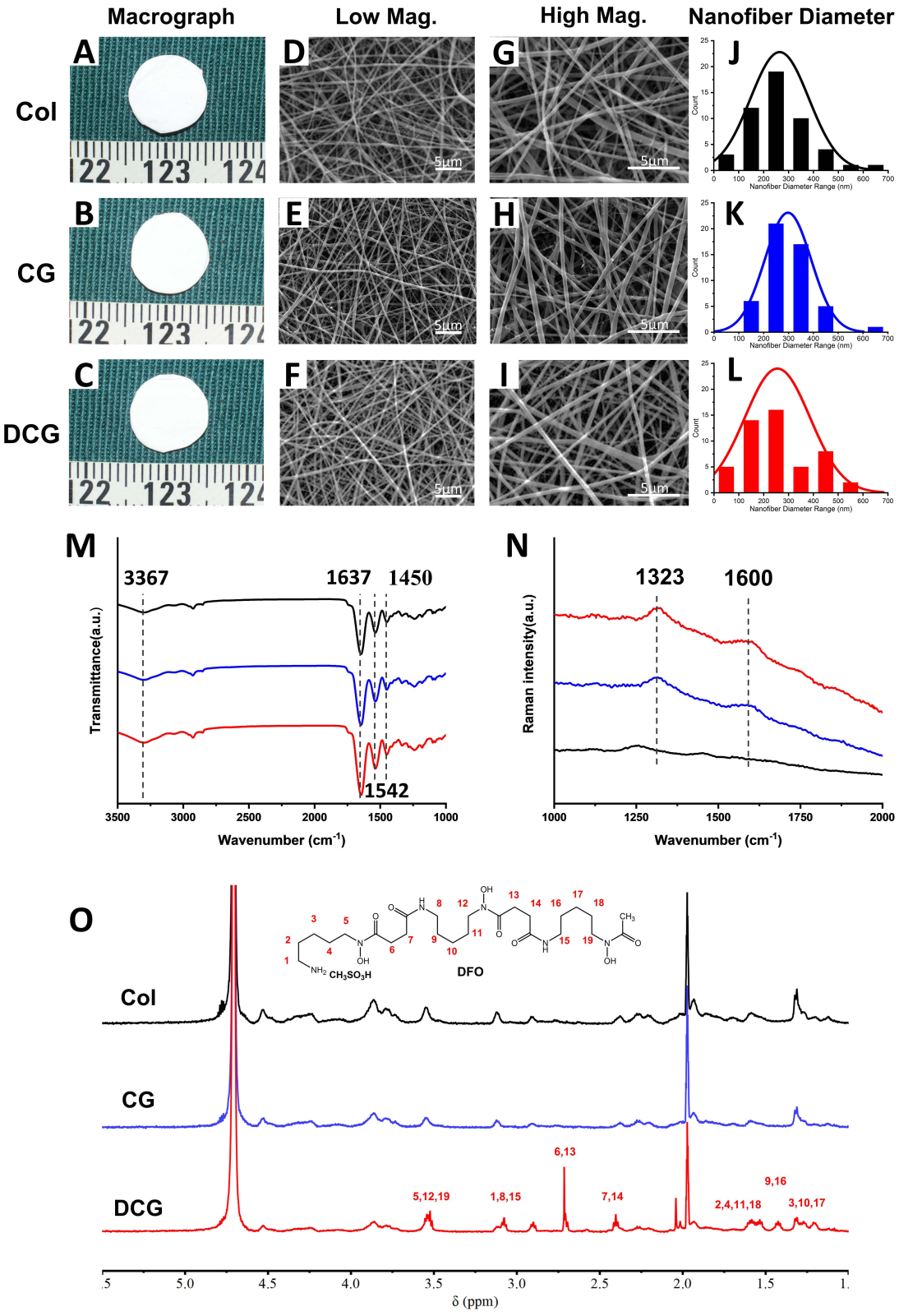

Figure 2 The morphology analysis and chemical properties of the DCG scaffolds. Macroscopic view of the (**A**) Col, (**B**) CG, and (**C**) DCG on the side view. SEM images of (**D, G**) Col, (**E, H**) CG, and (**F, I**) DCG on the side view. Distribution of nanofiber diameters within (**J**) Col, (**K**) CG, and (**L**) DCG. (**M**) ATR-FTIR spectra, (**N**) Raman spectra, and (**O**) 1H NMR spectrum.

Raman spectroscopy was performed to identify the GO in DCG scaffolds; it is a highly sensitive method for the detection of conjugated and double carbon–carbon bonds. The Raman spectroscopy (Figure 2N) displayed two evident peaks representing the G band at 1600 cm^{-1} and the D band at 1323 cm^{-1} respectively, which derived from in-plane vibrations of sp^2 carbon atoms of the graphite lattice and the out-of-plane breathing mode of the sp^2 atoms. With these observations, the presence of GO in the samples was verified.

The ^1H NMR spectra of the samples are shown in Figure 2O. Compared to the spectra of Col and CG, there were some new peaks in the spectra of DCG, which were consistent with the characteristic peaks of DFO reported in previous studies.[40] The signals at 2.0 and 2.8 ppm are respectively assigned to the protons of $-CH_3$ groups and $-CH_3SO_3H$, and those at 1.2–3.5 ppm is assigned to individual hydrogen atoms labeled in the spectrum of the DFO. This confirmed DFO as a component of the composite samples.

The water contact angles of the different nanofiber membranes are shown in Figure 3A and B. Among the scaffolds, the Col sample exhibited the highest angle value (65±2.434°), CG samples (62±1.384°), and DCG samples (61±2.711°), and the angle values of the Col group, CG group, and DCG group were statistically significant. Hence, for each of the sample types, the average water contact angle is below 70°, indicating their hydrophilic nature.[41] Furthermore, the addition of moderate concentrations of GO contributed to enhanced hydrophilicity in CG and DCG samples, as indicated

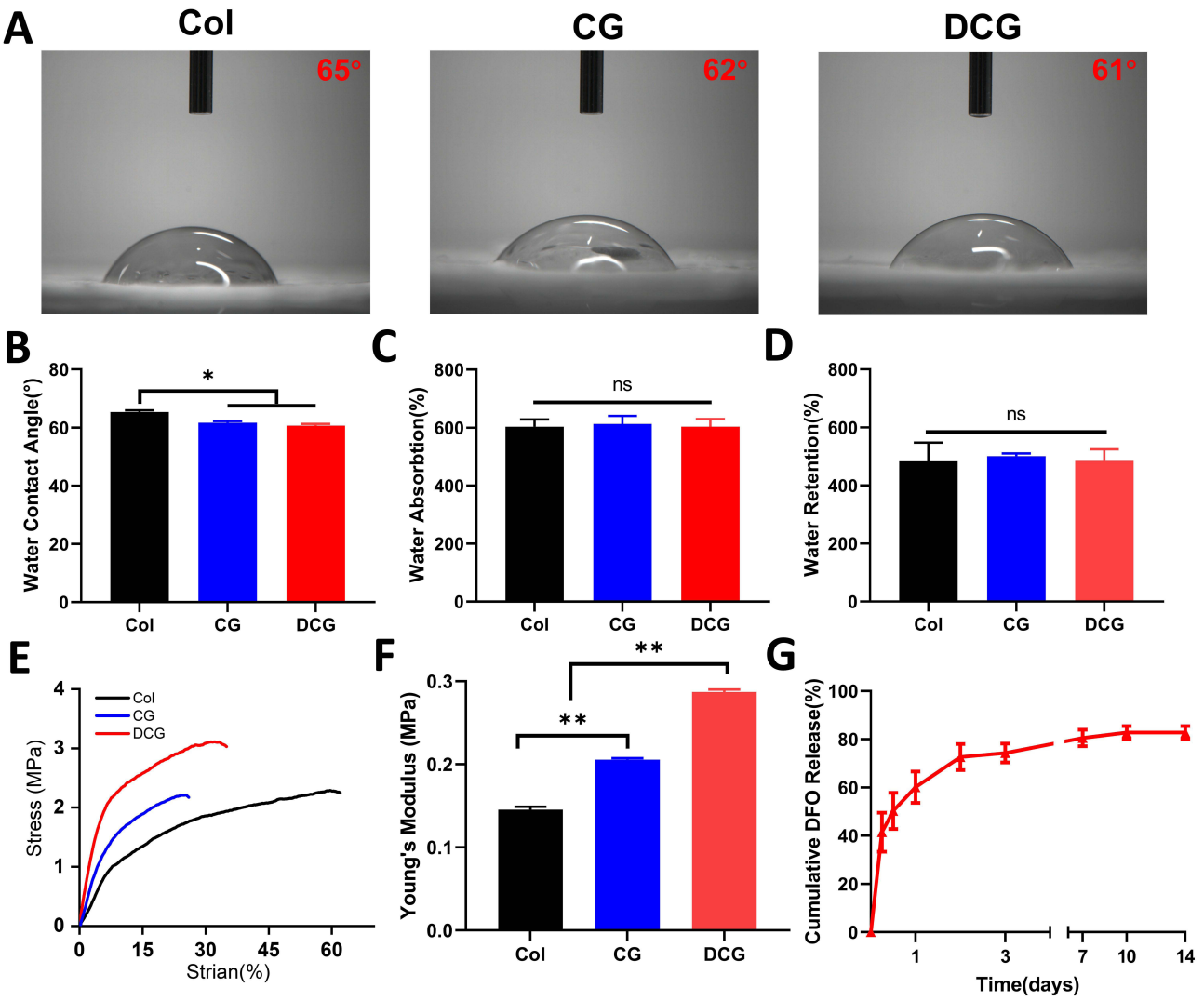

Figure 3 Physical characterization and drug release capacity of the DFO-Col-GO scaffolds. (**A**) Water contact angles. (**B**) Water contact angle statistics chart. (**C**) Water absorption, (**D**) water retention. (**E**) Stress-strain curves. (**F**) Young's moduli of the scaffolds. (**G**) Cumulative DFO release profiles. (*p < 0.05, **p < 0.01).

by their lower water contact angles relative to the Col sample. This might be the result of GO exhibiting hydrophilic characteristics due to the hydroxyl (OH) and carboxyl (COOH) functional groups.

As they exert a crucial role in cell ingrowth and metabolite circulation within the scaffolds, the water absorption and retention rates of the scaffolds were evaluated (Figure 3C and D). The water absorption rates of DCG, CG, and Col were 603.4±25, 612.6±28, and 602.9±26, respectively. Meanwhile, the water retention rates of each group were 483.1±64, 501.2±9, and 484.4±40, respectively. The results of water retention and water absorption of all groups showed no significant statistical difference, showing good water retention and water absorption performance.

The stress-strain curves of the different scaffolds are shown in Figure 3E. DCG had the highest tensile strength and the best flexibility, followed by CG, and Col. In Figure 3F, the graphs indicate an increase in Young's modulus with the addition of GO to Col to form CG, whereas DCG has the highest Young's modulus (0.2871±0.00292MPa) with maximum tensile stress, indicating that DCG has the best mechanical characteristics.

The DFO release profiles for the DCG scaffolds are shown in Figure 3G. The release of DFO on the first day is relatively rapid, about 60.15±6.53% of its total load in DCG. In the second stage, the release of DFO gradually slows down, reaching 74.26±3.97% on the 3rd day. The release rate further decreases over the following days and stabilizes from the tenth day with a final drug release rate of 82.77±2.72% on the 14th day.

Live and dead cell staining of scaffolds seeded with fibroblasts for 1, 3, and 5 days are shown in Figure 4A. Live cells displayed green fluorescence caused by Calcein AM staining while dead cells revealed a red fluorescence resulting from PI. With the extension of cell culture time, the density of green fluorescence in each group of samples gradually increased, with no obvious red fluorescence in any of them. There was no difference in the intensity of green fluorescence at each time point between each group. This supports the good cytocompatibility of both Col, CG, and DCG scaffolds. To quantify the cytotoxicity of the scaffolds in each group, we performed CCK8 assays on fibroblasts grown on samples from each group for 1, 3, and 5 days. The results of the experiments are shown in Figure 4B. The cells from each group of scaffolds demonstrated an obvious proliferation trend, with no significant difference between the groups as to cell viability at day 5, corroborating the findings from the live-dead cell staining.

To investigate the effect of in vitro angiogenesis of each group of scaffolds, we performed a tube formation assay on HUVECs using the extracts of each group of scaffolds, and the results are shown in Figure 5A. We found that HUVEC had more tube-like structures formed after incubation on Matrigel with DCG extract for 6 hours compared to the Col and CG groups. Statistical analysis was further carried out on the vascularization images and the mesh formation and junction formation by HUVECs cultured with different media are shown in Figure 5B and C, respectively. The number of meshes and nodes formed by the HUVECs cultured with DCG extract was 82.0±19.08 and 752.7±153.8, respectively. Compared to those formed by the HUVECs cultured with Col (19.33±7.37 and 250.7±74.78) and CG (25.67±4.04 and 334.7±22.5) extracts, there were significantly more meshes and nodes formed with the DCG extract ($P<0.01$).

RT-PCR was performed to assess the gene expression of HIF-1α and VEGF in HUVECs following culture with scaffolds' extracts. Results (Figure 5D and E) indicate that the DCG group induced the highest stimulatory effects on the gene expression of HIF-1α and VEGF in HUVECs, while the effects of Col did not significantly differ from those of CG.

The results of the cell migration assay using HUVECs are shown in Figure 6A. The DCG group had a faster wound healing rate with the smallest remaining wound area at 16h and 24h (Figure 6B). In the first 16 h, cells from the DCG group migrated faster, covering 62.9%±2.71% of the wound area compared to 25.8±7.09% for Col and 31.3±7.74% for CG. Similarly, at 24h, the DCG group maintained the highest cell migration rate, as 76.9 ± 6.29% of the scratched surface was repopulated with cells. In the Col and CG groups, only 48.1±10.56% and 50.3 ± 11.59% of the wounded area were closed then, respectively.

Figure 7A shows the images of diabetic wounds treated with different scaffolds for 0, 3, 7, 10, and 14 days post-surgery. From day 7 onwards, the wound area in the DCG group was significantly smaller than that in the Col and CG groups, while the wound area was similar between the Col and CG groups. On day 14, the wound in the DCG group had largely healed, whereas visible wounds remained in the Col and CG groups. Figure 7B shows the wound closure rate in each group. The DCG group had a much higher healing rate as compared with the Col and CG groups. The percentage of closed area for the DCG group was 95.07±1.8% and 99.49±1.03% on the 10th and 14th days, respectively, in comparison

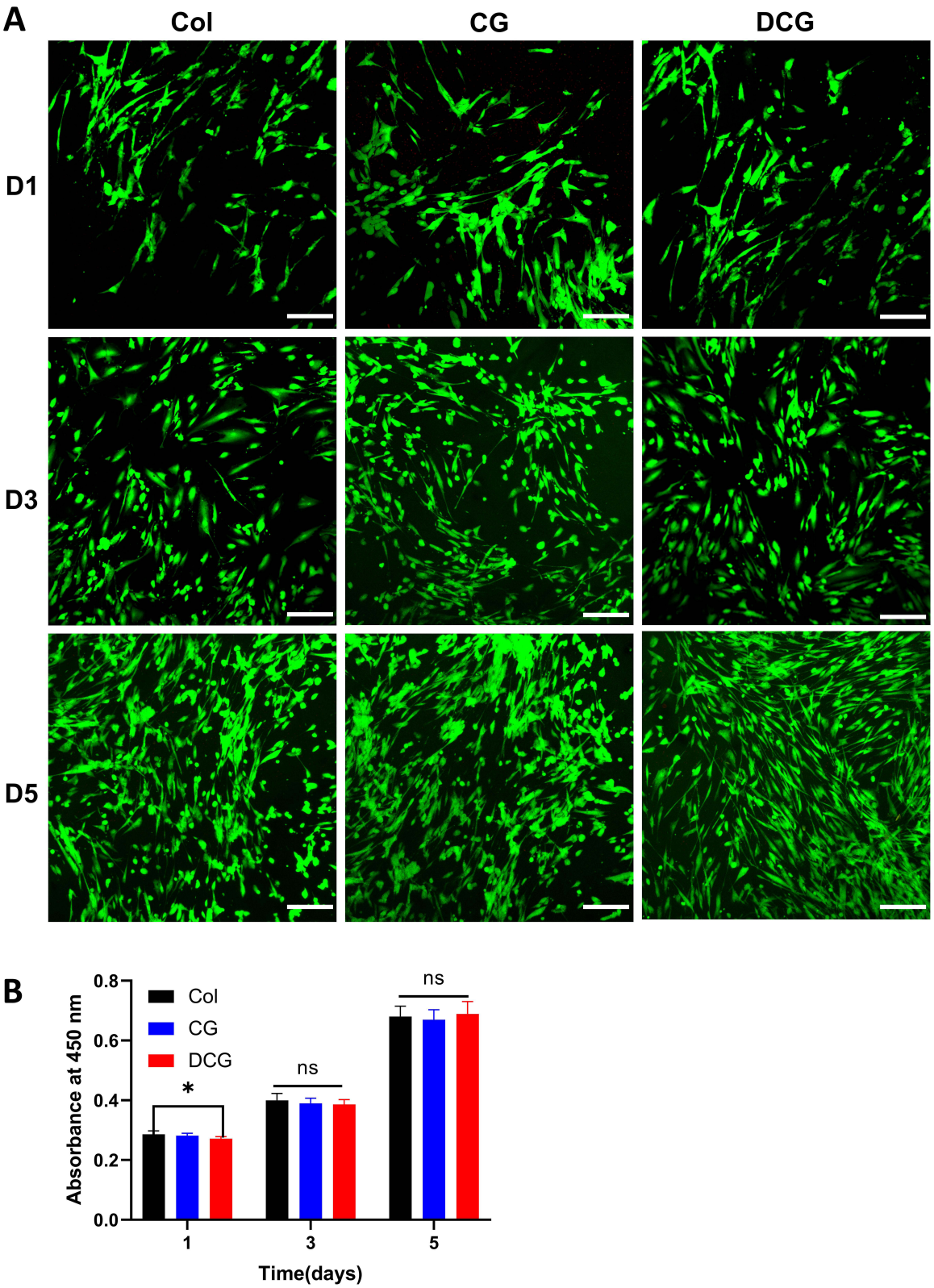

Figure 4 In vitro biocompatibility of the scaffolds. (**A**) Confocal fluorescent images for Calcein/PI staining of human dermal fibroblasts cultured on the scaffolds for 1, 3, and 5 days. (Scale bars: 200 μm). (**B**) Results of CCK-8 assay performed on human dermal fibroblasts seeded on the scaffolds. (*p < 0.05).

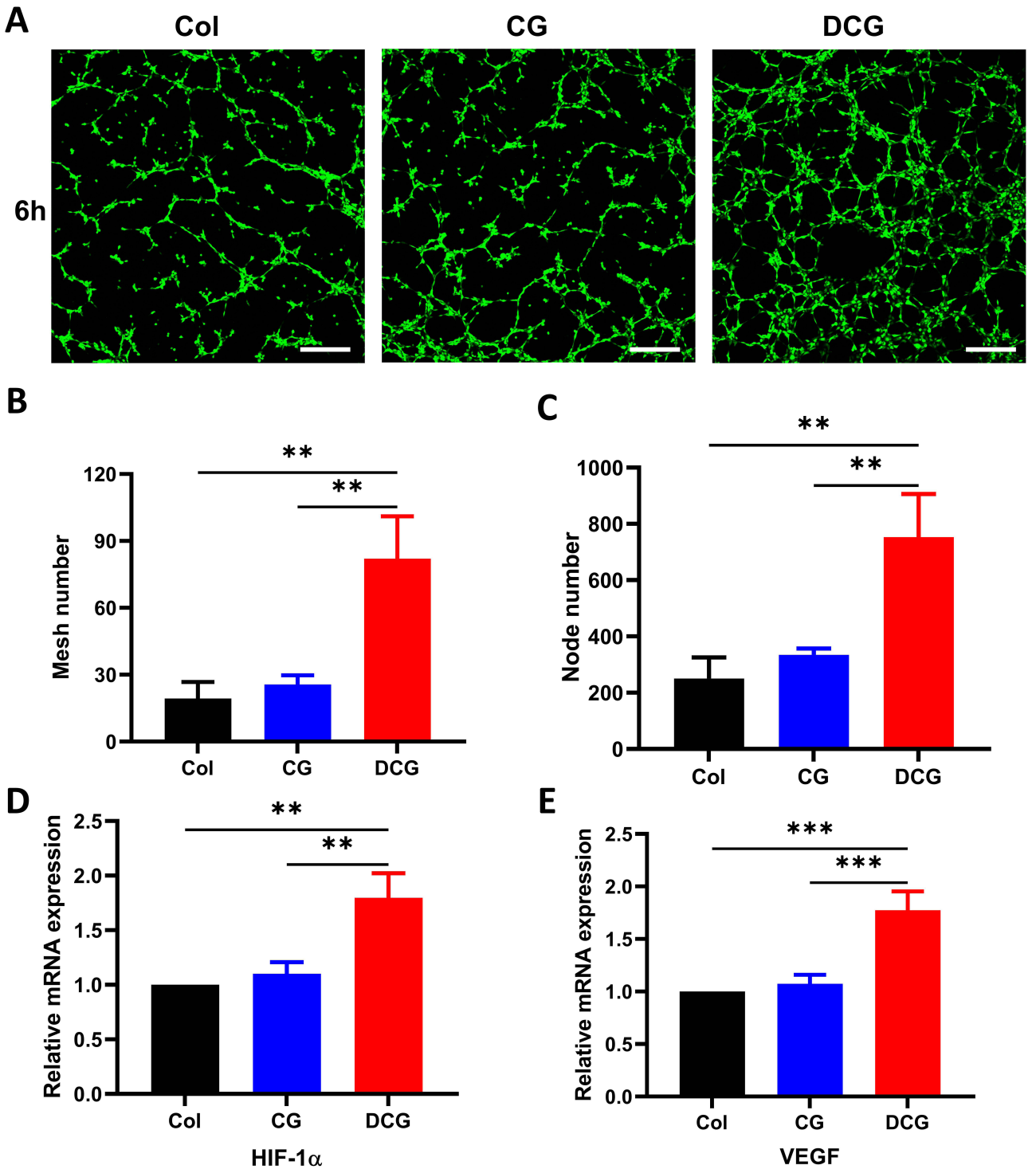

Figure 5 In vitro vascularization of GFP-HUVECs and relative mRNA expressions (**A**) Confocal fluorescent images from a Tube formation assay of GFP-HUVECs cultured by leaching solution of scaffolds after 6h. (Scale bars: 200 μm). (**B**) and (**C**) Quantitative analysis of meshes and nodes formed in the in vitro vascularization assay. (**D**) and (**E**) expression of HIF-1α and VEGF evaluated by PCR when GFP-HUVECs were cultured by leaching solution of scaffolds after 3 days. (**p < 0.01, ***p < 0.001).

with 73.49±6.37% and 68.58±11.8% on the 10th day, 84.84±5.09% and 84.71±5.05% on the 14th day for the Col and CG groups.

Histological studies were further carried out. Figure 7C shows images from H&E staining, with the black arrow and dotted line marking the unhealed area different in structure from normal skin tissue. On the 14th day after surgery, the

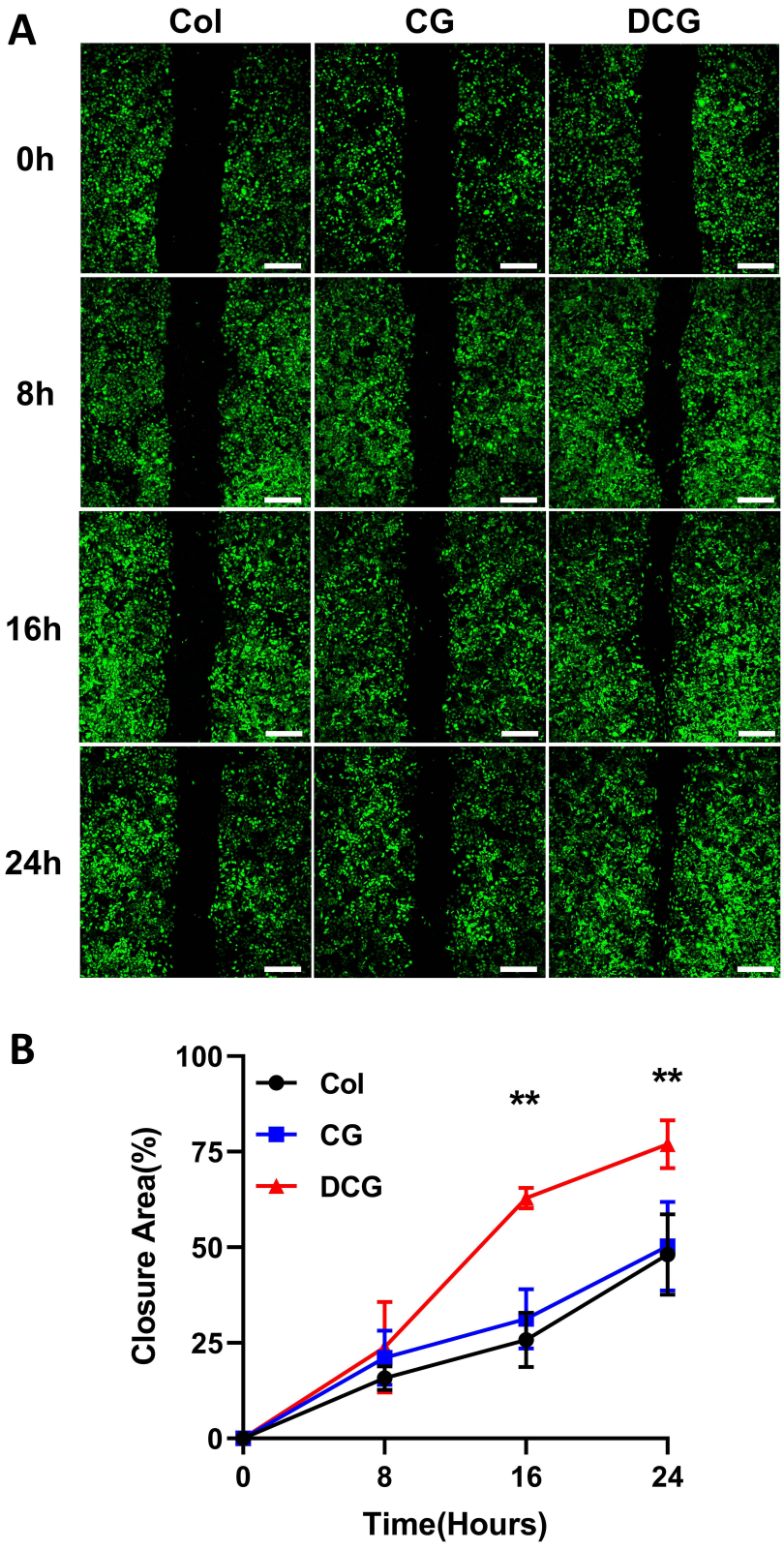

Figure 6 Scratch test of GFP-HUVECs. (**A**) Confocal fluorescent images from a scratch assay experiment at different time points. (Scale bars: 200 μm). (**B**) Closure area (%) of the Col, CG, and DCG at different time points. (**p < 0.01).

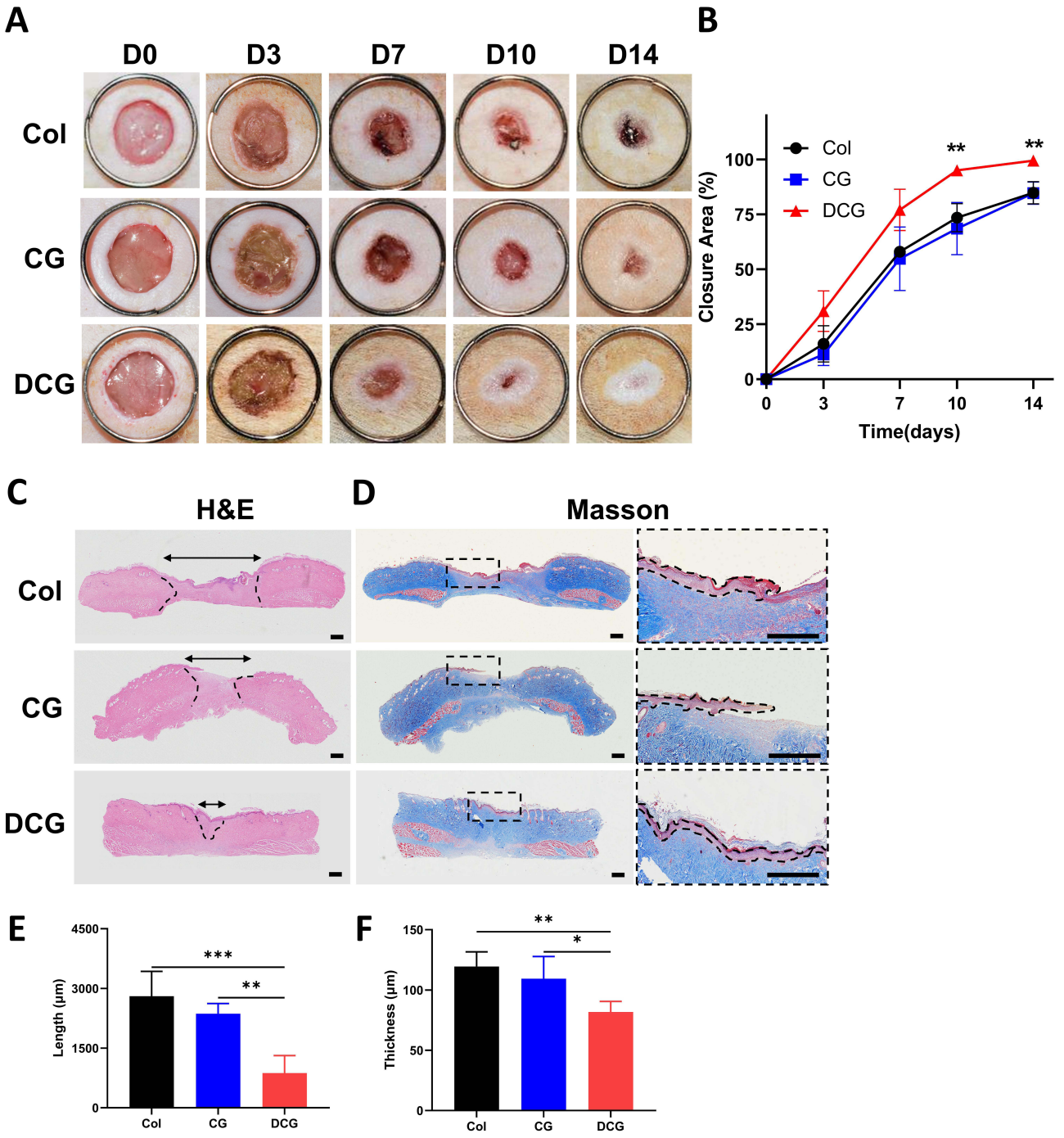

Figure 7 Effects of scaffolds in each group on wound healing in diabetic rats and histological analysis (**A**) Macroscopic views of the skin tissue sections at different time points after treatment. (**B**) Closure area (%) at different time points after treatment. (**C**) H&E staining and (**D**) Masson staining of wound section after 14 days of treatment. Black arrows: unhealed area (scale bars: 500 μm). A magnified view of the region shows the thickness of the epidermal layer indicated by dash lines (scale bars: 500 μm). The length of the unhealed area (**E**) and thickness of the epidermal layer (**F**) were analyzed. (*p < 0.05, **p < 0.01, ***p < 0.001).

Col and CG groups still presented remarkable tissue defects, where microstructure was disordered, and inflammatory cell infiltration was evident. The wound treated by DCG scaffolds had been repaired almost completely with a continuous epidermis, whereas the other groups resulted in defect healing with a discontinuous epidermis. Figure 7D shows Masson staining, where the DCG scaffold exhibited a uniform and thick collagen bundle deposition compared to other groups on the 14th day. Figure 7E was plotted for comparison of the unhealed wound length in different groups. The unhealed wound length for DCG (872.8±439.8μm) was shorter than that for Col (2805±624.6μm) and CG (2365±255.1μm).

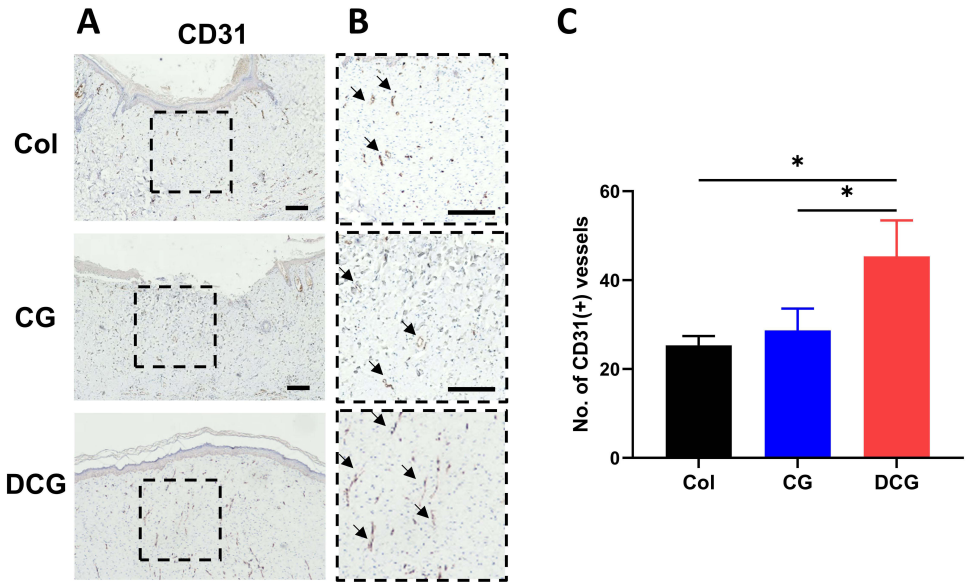

Figure 8 Immunohistochemical staining for CD31 in the DCG group compared with the other groups. (**A-B**) CD31 positive vascular endothelial cells were marked by black arrows (scale bars: 200 μm). (**C**) The number of CD31 positive vessels was analyzed. (*p < 0.05).

Figure 7F illustrates the thickness of the epidermis. The DCG group appeared with the best epidermal maturation marked by a uniform thickness (81.8±8.728μm). Col and CG on the other hand presented incomplete epithelization associated with a much thicker epidermal layer than that of DCG.

Immunohistochemical staining for CD31 is shown in Figure 8A and B. In the repair area, more angiogenesis was observed in the DCG group than in the Col and CG groups. Specifically, the number of blood capillaries in the DCG-treated group (45.33±8.08) was significantly higher than that in Col (25.33±2.08) and CG (28.67±8.08), as shown in Figure 8C, which was attributed to the pro-angiogenic effect of DFO.

Discussion

In patients with diabetes, poor wound healing due to hyperglycemia leads to the transition from an acute wound to a chronic wound. Due to the delay in diabetic wound healing, vascular damage caused by ischemia, and chronic inflammation leading to serious complications, life is at risk, so it is urgent to accelerate the healing of diabetic wounds.[42] In this study, we have fabricated DFO-loaded electrospun nanofiber scaffolds that facilitate the healing of diabetic wounds. The results showed that the DCG scaffolds have good physicochemical properties and biocompatibility, can release DFO sustainably over a therapeutically relevant time, upregulate the expression of HIF-1α and VEGF genes, promote angiogenesis, and accelerate the healing of diabetic rat wounds.

In the process of wound healing, angiogenesis within the new tissue is regulated by the HIF-1-α/VEGF axis.[43,44] In fact, in the early stages of wound healing after a skin injury, the expression of HIF-1α is increased in tissues at the wound edge, which stimulates the expression of VEGF.[45] Impairment of the HIF-1/VEGF axis, which results in defective neovascularization in response to hypoxia is one of the main causes of delayed wound healing in diabetic patients.[46] In diabetic wounds, under the influence of hyperglycemia, HIF-1α is degraded with the participation of Fe^{2+}, which interferes with the dimerization of HIF-1α into HIF-1β, resulting in reduced expression of downstream HIF-1 target genes such as VEGF and leading to insufficient VEGF protein expression, hindered angiogenesis and impaired wound healing.[47,48]

DFO is an FDA-approved small-molecule chelating chemical that removes iron by linking Fe^{2+} to its six hydroxyl groups, which prevents iron-catalyzed HIF-1α degradation, increases the transcription and expression of VEGF, and stimulates angiogenesis.[49] Herein, DFO has been extensively studied for promoting the healing of diabetic wounds. The study demonstrated the efficacy of DCG nanofiber scaffolds in stimulating angiogenesis and accelerating the healing of diabetic wounds. In the tube formation assay, more tubular structures were observed in the DCG group compared to the

Col and CG groups (Figure 5A), and the number of tubes and mesh were also higher (Figure 5B and C), which was mainly attributed to the angiogenic effect of DFO released from the DCG scaffold. Angiogenesis is initiated by endothelial cells' sprouting, as they proliferate and migrate in response to pro-angiogenic signals including VEGF.[43] The formation of new blood vessels is also facilitated by the accelerated migration of vascular endothelial cells. Since the DCG scaffold can release DFO (Figure 6A and B) to stimulate endothelial cells to express VEGF, the DCG-treated HUVECs exhibited stronger migration ability and faster cell migration rate, underlining more efficient sprouting and formation of vascular structures with DCG. However, the Col and CG groups failed to induce significant pro-angiogenic and pro-migration effects. Meanwhile, we confirmed by PCR that DCG can upregulate the expression of HIF-1α and VEGF in HUVECs through the activity of released DFO (Figure 5D and E), which is consistent with previous studies and further explains the mechanism of DCG in promoting angiogenesis and migration.[50] In the in vivo experiment, the DCG group had a faster healing trend on day 7 and approached complete healing on day 14, with a wound healing area percentage of 99.49±1.03% (Figure 7A and B). Histological staining statistics showed that the unhealed wound length in the DCG group was the shortest (872.8±439.8μm), the epidermal maturity was the best, and the thickness was uniform (81.8±8.728μm), which was better than that in other groups (Figure 7E and F). In addition, the immunohistochemical results of CD31 showed more angiogenesis in the DCG group (Figure 8A and B), among which the number of capillaries in the DCG group (45.33±8.08) was significantly better than that in the other groups (Figure 8C), indicating that DFO had obvious vascularization promoting ability. Interestingly, the new skin in the DCG group was further marked by reduced inflammatory cell infiltration and enhanced collagen deposition, probably because DFO reduces macrophage TNF-1α secretion and suppresses the inflammatory response.[15]

Subcutaneous administration of DFO at high dosages may lead to pain and swelling at the injection site, as well as ophthalmic, auditory, neurological, and renal deterioration.[11] Moreover, DFO has a short half-life of only 12 min, leading it to be rapidly metabolized by plasma enzymes.[51] To overcome such limitations, local and slow release of DFO over longer periods is necessary for application in therapeutics such as for diabetic wound treatment. Kong developed an injectable hydrogel containing DFO for enhanced repair of chronic diabetic skin defects with a slow release of DFO for more than 24 hours.[50] Although the hydrogel has good efficacy in accelerating wound healing, it requires replacing the hydrogel dressing every 3 days, and frequent wound dressing changes have been shown to cause pain, irritation, and increased risk of infection.[16] Electrospun nanofiber scaffolds with high specific surface area and porous structure like ECM have a wide range of applications in drug delivery, tissue engineering and regenerative medicine.[52,53] A nanofiber scaffold may be a preferable way to sustainably deliver DFO. In situ application of nanofibrous scaffolds could minimize the disadvantages of systemic perfusion with the free drug, and on the other hand maximize the drug pharmaceutical effects by a controlled and sustained release directly at the site of action.[54] Chen et al prepared a PCL-chitosan nanofiber scaffold that can sustainably release DFO for up to 72 hours.[48] GO is a promising nanocarrier for drug delivery systems due to its large surface to volume ratio and stability.[55] -COOH and -OH functional groups present in GO allow for strong hydrogen bond interactions to take place with the free amino groups in DFO, which improves drug loading efficiency. In our study, DCG can release DFO rapidly in the first 24 h to compensate for the short half-life of DFO, and release DFO slowly and continuously in the subsequent time to maintain the traumatic DFO concentration at a certain level for 14 days, reducing the number of dressing changes (Figure 3G).

Nanofiber scaffolds have been widely used as wound dressings due to their drug-loading capacity and good biocompatibility.[56] Col, the most abundant component of skin ECM, has excellent biocompatibility is non-biotoxic, and is often used to prepare diabetic wound dressings.[57,58] Long et al found that the functionalization of collagen by VEGF and SDF-1 containing collagen-binding domains could coordinate angiogenesis and inflammation for diabetic wound healing.[59] However, pure collagen scaffolds' application is constrained by poor mechanical properties and a lack of biological activity.[21] The incorporation of GO into collagen can significantly improve the mechanical properties of the scaffold, but there is obvious cytotoxicity when GO concentration is higher than 1%.[60,61] Our previous study found that the Col nanofiber scaffold with 0.2%w/w GO had the best mechanical properties, and there was no significant difference from the pure Col scaffold in biocompatibility.[62] In this study, we once again confirmed that the addition of GO would not affect the biocompatibility of Col (Figure 4A and B). Importantly, DCG scaffolds loaded with DFO also showed good biocompatibility without obvious cytotoxicity and had higher elastic modulus in DCG scaffolds containing DFO

(Figure 3F). The results showed that DCG had a better ability to resist external deformation while maintaining good cytocompatibility. In addition, the ideal wound dressing needs to have good hydrophilicity, high-water absorption, and water retention. All scaffolds had the same high-water absorption rate and water retention rate (Figure 3C and D), which might be due to the similar porosity among the groups. However, because GO is rich in hydrophilic groups,[63] such as -COOH and -OH, CG and DCG showed higher hydrophilicity (Figure 3A and B). A high hydrophilic surface promotes cell adhesion, proliferation, and penetration, which is beneficial to wound healing,[41] On the other hand, the high-water absorption rate and water retention rate can absorb the wound exudate while maintaining the local moist microenvironment of the wound, which is conducive to the formation of granulation tissue.[64]

Conclusions

We have successfully constructed a Col-GO nanofiber scaffold (DCG) loaded with DFO by electrospinning technology. The scaffold has good hydrophilic properties, mechanical properties, drug release properties, and biocompatibility. The release of the DFO drug promotes angiogenesis by upregulating the expression of HIF-1α and VEGF genes. In addition, the scaffold can not only promote full-thickness wound repair in diabetic rats but also promote vascularization ability in vivo. The scaffold provides a new option for promoting full-thickness wound repair in diabetic rats.

Ethics Approval and Consent to Participate

Number [2019] IEC (S1154) was approved by Experimental Animal Ethics Committee of Huazhong University of Science and Technology for the studies involving animal.

Acknowledgments

The authors wish to appreciate the Analytical & Testing Center of Huazhong University of Science and Technology and the help from Zhijun Chen of Wuhan Textile University.

Funding

This research was supported by the National Key Research and Development Program of China (No: 2019YFA0110500), the National Natural Science Foundation of China (No: 81501674, 82102351, 82272286), and the Provincial Natural Science of Hubei (No: 2018CFB489).

Disclosure

The authors declare no competing interests in this work.

References

1. Zheng Y, Ley SH, Hu FB. Global aetiology and epidemiology of type 2 diabetes mellitus and its complications. *Nat Rev Endocrinol*. 2018;14(2):88–98. doi:10.1038/nrendo.2017.151
2. Liang Y, Li M, Yang Y, et al. Ph/glucose dual responsive metformin release hydrogel dressings with adhesion and self-healing via dual-dynamic bonding for athletic diabetic foot wound healing. *ACS Nano*. 2022;16(2):3194–3207. doi:10.1021/acsnano.1c11040
3. Armstrong DG, Boulton AJM, Bus SA. Diabetic foot ulcers and their recurrence. *N Engl J Med*. 2017;376(24):2367–2375. doi:10.1056/NEJMra1615439
4. Shao Z, Yin T, Jiang J, et al. Wound microenvironment self-adaptive hydrogel with efficient angiogenesis for promoting diabetic wound healing. *Bioact Mater*. 2023;20:561–573. doi:10.1016/j.bioactmat.2022.06.018
5. Tu Z, Chen M, Wang M, et al. Engineering bioactive m2 macrophage-polarized anti-inflammatory, antioxidant, and antibacterial scaffolds for rapid angiogenesis and diabetic wound repair. *Adv Funct Mater*. 2021;31(30):2100924. doi:10.1002/adfm.202100924
6. Zheng X, Narayanan S, Sunkari VG, et al. Triggering of a dll4–notch1 loop impairs wound healing in diabetes. *Proc Natl Acad Sci*. 2019;116(14):6985–6994. doi:10.1073/pnas.1900351116
7. Niu Y, Li Q, Ding Y, Dong L, Wang C. Engineered delivery strategies for enhanced control of growth factor activities in wound healing. *Adv Drug Deliv Rev*. 2019;146:190–208. doi:10.1016/j.addr.2018.06.002
8. Okonkwo UA, DiPietro LA. Diabetes and wound angiogenesis. *Int J Mol Sci*. 2017;18(7):1419. doi:10.3390/ijms18071419
9. Glotzbach JP, Wong VW, Gurtner GC. Neovascularization in diabetes. *Expert Rev Endocrinol Metab*. 2010;5(1):99–111. doi:10.1586/eem.09.57
10. Li G, Ko CN, Li D, et al. A small molecule hif-1α stabilizer that accelerates diabetic wound healing. *Nat Commun*. 2021;12(1):3363. doi:10.1038/s41467-021-23448-7
11. Tchanque-Fossuo C, Dahle S, Buchman S, Rivkah Isseroff R. Deferoxamine: potential novel topical therapeutic for chronic wounds. *British Journal of Dermatology*. 2017;176(4):1056–1059. doi:10.1111/bjd.14956

12. Duscher D, Trotsyuk AA, Maan ZN, et al. Optimization of transdermal deferoxamine leads to enhanced efficacy in healing skin wounds. *J Control Release*. 2019;308:232–239. doi:10.1016/j.jconrel.2019.07.009
13. Zheng X, Zhang X, Wang Y, et al. Hypoxia-mimicking 3d bioglass-nanoclay scaffolds promote endogenous bone regeneration. *Bioact Mater*. 2021;6(10):3485–3495. doi:10.1016/j.bioactmat.2021.03.011
14. Han X, Sun M, Chen B, et al. Lotus seedpod-inspired internal vascularized 3d printed scaffold for bone tissue repair. *Bioact Mater*. 2021;6(6):1639–1652. doi:10.1016/j.bioactmat.2020.11.019
15. Ding Z, Zhang Y, Guo P, et al. Injectable desferrioxamine-laden silk nanofiber hydrogels for accelerating diabetic wound healing. *ACS Biomater Sci Eng*. 2021;7(3):1147–1158. doi:10.1021/acsbiomaterials.0c01502
16. Li N, Zhan A, Jiang Y, Liu H. A novel matrix metalloproteinases-cleavable hydrogel loading deferoxamine accelerates diabetic wound healing. *Int J Biol Macromol*. 2022;222(Pt A):1551–1559. doi:10.1016/j.ijbiomac.2022.09.185
17. Shoulders MD, Raines RT. Collagen structure and stability. *Annu Rev Biochem*. 2009;78(1):929–958. doi:10.1146/annurev.biochem.77.032207.120833
18. Hernández-Rangel A, Martin-Martinez ES. Collagen based electrospun materials for skin wounds treatment. *J Biomed Mater Res A*. 2021;109(9):1751–1764. doi:10.1002/jbm.a.37154
19. Levingstone TJ, Ramesh A, Brady RT, et al. Cell-free multi-layered collagen-based scaffolds demonstrate layer specific regeneration of functional osteochondral tissue in caprine joints. *Biomaterials*. 2016;87:69–81. doi:10.1016/j.biomaterials.2016.02.006
20. Sharma S, Rai VK, Narang RK, Markandeywar TS. Collagen-based formulations for wound healing: a literature review. *Life Sci*. 2022;290:120096. doi:10.1016/j.lfs.2021.120096
21. Cholas R, Kunjalukkal Padmanabhan S, Gervaso F, et al. Scaffolds for bone regeneration made of hydroxyapatite microspheres in a collagen matrix. *Mater Sci Eng C Mater Biol Appl*. 2016;63:499–505. doi:10.1016/j.msec.2016.03.022
22. Chen H, Müller MB, Gilmore KJ, Wallace GG, Li D. Mechanically strong, electrically conductive, and biocompatible graphene paper. *Adv Mater*. 2008;20(18):3557–3561. doi:10.1002/adma.200800757
23. Zhang Q, Du Q, Zhao Y, et al. Graphene oxide-modified electrospun polyvinyl alcohol nanofibrous scaffolds with potential as skin wound dressings. *RSC Adv*. 2017;7(46):28826–28836. doi:10.1039/C7RA03997B
24. Khorshidi S, Mohebbali M, Imani R, Mahmoodi M, Solouk A. Electrospun fibroin/graphene oxide nanocomposite mats: an optimization for potential wound dressing applications. *Fibers Polym*. 2020;21(3):480–488. doi:10.1007/s12221-020-9465-z
25. Song J, Gao H, Zhu G, et al. The preparation and characterization of polycaprolactone/graphene oxide biocomposite nanofiber scaffolds and their application for directing cell behaviors. *Carbon*. 2015;95:1039–1050. doi:10.1016/j.carbon.2015.09.011
26. Audtarat S, Hongsachart P, Dasri T, et al. Green synthesis of silver nanoparticles loaded into bacterial cellulose for antimicrobial application. *Nanocomposites*. 2022;8(1):34–46. doi:10.1080/20550324.2022.2055375
27. Yang Y, Zhang R, Liang Z, et al. Application of electrospun drug-loaded nanofibers in cancer therapy. *Polymers*. 2024;16(4):504.
28. Bai Y, Liu Y, Lv H, et al. Processes of electrospun polyvinylidene fluoride-based nanofibers, their piezoelectric properties, and several fantastic applications. *Polymers*. 2022;14(20):4311. doi:10.3390/polym14204311
29. Mouro C, Gomes AP, Ahonen M, Fangueiro R, Gouveia IC. Chelidoniummajus l. Incorporated emulsion electrospun pcl/pva_pec nanofibrous meshes for antibacterial wound dressing applications. *Nanomaterials*. 2021;11(7):1785. doi:10.3390/nano11071785
30. Dinuwan Gunawardhana KRS, Simorangkir R, McGuinness GB, et al. The potential of electrospinning to enable the realization of energy-autonomous wearable sensing systems. *ACS Nano*. 2024;18(4):2649–2684. doi:10.1021/acsnano.3c09077
31. Gong W, Yang W, Zhou J, et al. Engineered beads-on-a-string nanocomposites for an improved drug fast-sustained bi-stage release. *Nanocomposites*. 2024;10(1):240–253. doi:10.1080/20550324.2024.2362477
32. Chen X, Liu Y, Liu P. Electrospun core-sheath nanofibers with a cellulose acetate coating for the synergistic release of zinc ion and drugs. *Mol Pharm*. 2024;21(1):173–182. doi:10.1021/acs.molpharmaceut.3c00703
33. Yan S, Qian Y, Haghayegh M, et al. Electrospun organic/inorganic hybrid nanofibers for accelerating wound healing: a review. *J Mater Chem B*. 2024;12(13):3171–3190. doi:10.1039/D4TB00149D
34. Zhao P, Zhou K, Xia Y, et al. Electrospun trilayer eccentric janus nanofibers for a combined treatment of periodontitis. *Adv Fiber Mater*. 2024;6(4):1053–1073. doi:10.1007/s42765-024-00397-6
35. Zhang X, Yu N, Ren Q, et al. Janus nanofiber membranes with photothermal-enhanced biofluid drainage and sterilization for diabetic wounds. *Adv Funct Mater*. 2024;34(24):2315020.
36. Si Y, Shi S, Hu J. Applications of electrospinning in human health: from detection, protection, regulation to reconstruction. *Nano Today*. 2023;48:101723. doi:10.1016/j.nantod.2022.101723
37. Huang Z, An H, Guo H, et al. An asymmetric natural nanofiber with rapid temperature responsive detachability inspired by Andrias davidianus for full-thickness skin wound healing. *Adv Fiber Mater*. 2024;6(2):473–488. doi:10.1007/s42765-023-00364-7
38. Xue J, Pisignano D, Xia Y. Maneuvering the migration and differentiation of stem cells with electrospun nanofibers. *Adv Sci*. 2020;7(15):2000735. doi:10.1002/advs.202000735
39. Vignesh S, Sivashanmugam A, Annapoorna M, et al. Injectable deferoxamine nanoparticles loaded chitosan-hyaluronic acid coacervate hydrogel for therapeutic angiogenesis. *Colloids Surf B Biointerfaces*. 2018;161:129–138. doi:10.1016/j.colsurfb.2017.10.033
40. Tian M, Chen X, Gu Z, et al. Synthesis and evaluation of oxidation-responsive alginate-deferoxamine conjugates with increased stability and low toxicity. *Carbohydr Polym*. 2016;144:522–530. doi:10.1016/j.carbpol.2016.03.014
41. Ahn S, Ardona HAM, Campbell PH, Gonzalez GM, Parker KK. Alfalfa nanofibers for dermal wound healing. *ACS Appl Mater Interfaces*. 2019;11(37):33535–33547. doi:10.1021/acsami.9b07626
42. Razzaq A, Khan ZU, Saeed A, et al. Development of cephradine-loaded gelatin/polyvinyl alcohol electrospun nanofibers for effective diabetic wound healing: in-vitro and in-vivo assessments. *Pharmaceutics*. 2021;13(3):349. doi:10.3390/pharmaceutics13030349
43. Rodrigues M, Kosaric N, Bonham CA, Gurtner GC. Wound healing: a cellular perspective. *Physiol Rev*. 2019;99(1):665–706. doi:10.1152/physrev.00067.2017
44. Botusan IR, Sunkari VG, Savu O, et al. Stabilization of hif-1alpha is critical to improve wound healing in diabetic mice. *Proc Natl Acad Sci*. 2008;105(49):19426–19431. doi:10.1073/pnas.0805230105

45. Elson DA, Ryan HE, Snow JW, Johnson R, Arbeit JM. Coordinate up-regulation of hypoxia inducible factor (hif)-1alpha and hif-1 target genes during multi-stage epidermal carcinogenesis and wound healing. *Cancer Res*. 2000;60(21):6189–6195.
46. Zhu Y, Wang Y, Jia Y, Xu J, Chai Y. Roxadustat promotes angiogenesis through HIF-1α/VEGF/VEGFR2 signaling and accelerates cutaneous wound healing in diabetic rats. *Wound Repair Regen*. 2019;27(4):324–334. doi:10.1111/wrr.12708
47. Davis FM, Kimball A, Boniakowski A, Gallagher K. Dysfunctional wound healing in diabetic foot ulcers: new crossroads. *Curr Diab Rep*. 2018;18 (1):2. doi:10.1007/s11892-018-0970-z
48. Chen H, Jia P, Kang H, et al. Upregulating hif-1α by hydrogel nanofibrous scaffolds for rapidly recruiting angiogenesis relative cells in diabetic wound. *Adv Healthc Mater*. 2016;5(8):907–918. doi:10.1002/adhm.201501018
49. Holden P, Nair LS. Deferoxamine: an angiogenic and antioxidant molecule for tissue regeneration. *Tissue Eng Part B Rev*. 2019;25(6):461–470. doi:10.1089/ten.teb.2019.0111
50. Kong L, Wu Z, Zhao H, et al. Bioactive injectable hydrogels containing desferrioxamine and bioglass for diabetic wound healing. *ACS Appl Mater Interfaces*. 2018;10(36):30103–30114. doi:10.1021/acsami.8b09191
51. Duscher D, Neofytou E, Wong VW, et al. Transdermal deferoxamine prevents pressure-induced diabetic ulcers. *Proc Natl Acad Sci*. 2015;112 (1):94–99. doi:10.1073/pnas.1413445112
52. Khan NU, Chengfeng X, Jiang MQ, et al. Obstructed vein delivery of ceftriaxone via poly(vinyl-pyrrolidone)-iodine-chitosan nanofibers for the management of diabetic foot infections and burn wounds. *Int J Biol Macromol*. 2024;277(Pt 2):134166. doi:10.1016/j.ijbiomac.2024.134166
53. Song J, Razzaq A, Khan NU, Iqbal H, Ni J. Chitosan/poly (3-hydroxy butyric acid-co-3-hydroxy valeric acid) electrospun nanofibers with cephradine for superficial incisional skin wound infection management. *Int J Biol Macromol*. 2023;250:126229. doi:10.1016/j.ijbiomac.2023.126229
54. Narayanaswamy R, Torchilin VP. Hydrogels and their applications in targeted drug delivery. *Molecules*. 2019;24(3):603. doi:10.3390/molecules24030603
55. Prabakaran S, Jeyaraj M, Nagaraj A, Sadasivuni KK, Rajan M. Polymethyl methacrylate–ovalbumin@ graphene oxide drug carrier system for high anti-proliferative cancer drug delivery. *Appl Nanosci*. 2019;9(7):1487–1500. doi:10.1007/s13204-019-00950-5
56. Kamal R, Razzaq A, Ali Shah K, et al. Evaluation of cephalexin-loaded phbv nanofibers for mrsa-infected diabetic foot ulcers treatment. *J Drug Deliv Sci Technol*. 2022;71:103349.
57. Shen T, Dai K, Yu Y, Wang J, Liu C. Sulfated chitosan rescues dysfunctional macrophages and accelerates wound healing in diabetic mice. *Acta Biomater*. 2020;117:192–203. doi:10.1016/j.actbio.2020.09.035
58. Zhang L, Zhou Y, Su D, et al. Injectable, self-healing and ph responsive stem cell factor loaded collagen hydrogel as a dynamic bioadhesive dressing for diabetic wound repair. *J Mater Chem B*. 2021;9(29):5887–5897. doi:10.1039/D1TB01163D
59. Long G, Liu D, He X, et al. A dual functional collagen scaffold coordinates angiogenesis and inflammation for diabetic wound healing. *Biomater Sci*. 2020;8(22):6337–6349. doi:10.1039/D0BM00999G
60. Liu J, Hou J, Liu S, et al. Graphene oxide functionalized double-layered patch with anti-adhesion ability for abdominal wall defects. *Int J Nanomed*. 2021;16:3803–3818. doi:10.2147/IJN.S312074
61. Faraji S, Nowroozi N, Nouralishahi A, Shabani Shayeh J. Electrospun poly-caprolactone/graphene oxide/quercetin nanofibrous scaffold for wound dressing: evaluation of biological and structural properties. *Life Sci*. 2020;257:118062. doi:10.1016/j.lfs.2020.118062
62. Chen J, Zhang G, Zhao Y, et al. Promotion of skin regeneration through co-axial electrospun fibers loaded with basic fibroblast growth factor. *Adv Compos Hybrid Mater*. 2022;1–15.
63. Aidun A, Safaei Firoozabady A, Moharrami M, et al. Graphene oxide incorporated polycaprolactone/chitosan/collagen electrospun scaffold: enhanced osteogenic properties for bone tissue engineering. *Artif Organs*. 2019;43(10):E264–E281. doi:10.1111/aor.13474
64. Sumayya A, Muraleedhara Kurup G. Marine macromolecules cross-linked hydrogel scaffolds as physiochemically and biologically favorable entities for tissue engineering applications. *J biomater sci Poly ed*. 2017;28(9):807–825. doi:10.1080/09205063.2017.1303119